Synchronization of pendula rotating in different directions

Krzysztof Czolczynski, Przemysław Perlikowski, Andrzej Stefanski and Tomasz Kapitaniak

Division of Dynamics, Technical University of Lodz, Stefanowskiego 1/15,

90-924 Lodz, Poland

Abstract: We study the synchronization of a number of pendula mounted on a horizontal beam which can roll on the parallel surface. Under the driving moment, the pendula rotate in different directions: one of them rotates counterclockwise, the rest rotate clockwise. It has been shown that after a transient different types of phase synchronization between pendula can be observed, despite opposite directions of rotations.

1. Introduction

Mechanical systems that contain rotating parts (for example vibro-exciters, unbalance rotors) are typical in engineering applications and for years have been the subject of intensive studies [1-3]. One problem of scientific interest, which among others occurs in such systems is the phenomenon of synchronization of different rotating parts [4,5 and references within]. Despite different initial conditions, after a sufficiently long transient, the rotating parts move in the same way - complete synchronization, or a permanent constant shift is established between their displacements, i.e., the angles of rotation - phase synchronization [6-8]. Synchronization occurs due to dependence of the periods of rotating elements motion and the displacement of the base on which these elements are mounted [9]. Prasad [10] considers the system of coupled counter-rotating oscillators and observes a mixed synchronizations, i.e., some systems' variables are synchronized in-phase, while others are out-of-phase.

Recently, the rotational motions of the pendulum attracted more interest due to the concept of extracting energy from sea waves using pendulum dynamics proposed by Wiercigroch [11]. The examples of such studies can be found in [12-19]. This interest motivated us to pose the question; under which condition can slowly rotating pendula synchronize.

In the previous paper [20] we consider the dynamics of the system consisting of n pendula mounted on the movable beam. The pendula are excited by the external torques which are inversely proportional to the angular velocities of the pendula. As the result of such excitation each pendulum rotates around its axis of rotation. It has been assumed that all pendula rotate in the same direction. We consider the case of slowly rotating pendulums and consider the influence of the gravity on their motion. It has been shown that both complete and phase synchronizations of the rotating pendula are possible. We derive the approximate analytical conditions for both types of synchronizations and equations which allow the estimation of the phase differences between the pendula. Contrary to the case of oscillatory pendulums [21,22] phase synchronization is not limited to three and five clusters configurations. Our results have been compared to these of [4].

In this paper we study the dynamics of the similar system as in [20] but this time we assume that one pendulum (numbered 1) rotates counterclockwise, i.e., has a positive angular velocity angular while the remaining pendula rotates clockwise with negative angular

velocity. We consider two cases: (i) pendula rotate in the horizontal plane, i.e., the gravity has no influence on their motion, (ii) pendula rotate in the vertical plane and the weight of them causes the unevenness of their rotation, i.e., the pendula slow down when the center of its mass goes up and accelerates when the center of its mass goes down. We show that in such systems, despite opposite directions of rotation different types of synchronization occur. We give evidence that our results are robust as they exist in the wide range of system parameters.

The paper is organized as follows. In Sec.2 we describe the considered model of the coupled rotating pendulums. Section 3 presents the analytical studies which allow to derive the synchronization condition. The examples of the configurations of the synchronized pendulums are given in Sec. 4. Finally, we summarize our results in Sec. 5.

2. The model

We consider the system shown in Figure 1. It consists of a rigid beam of mass M on which n identical rotating pendula are mounted. The beam is connected to a stationary base by the spring with a stiffness coefficient k_x and a damper with a damping coefficient c_x. Due to the existence of the forces of inertia, which act on each pendulum pivot, the beam can move in the horizontal direction (this motion is described by coordinate x). The masses of the pendula are indicated as m. B is the moment of inertia with respect to the axis of rotation. l is the distance from the axis of rotation to the center of the pendulum's mass. Rotation of the i-th pendula is described by φ_i. The rotations of the pendula are damped by linear dampers (not shown in Figure 1) with damping coefficient c_φ. Each pendulum is driven by the drive moment inversely proportional to their velocity: $N_{0i} - \dot{\varphi}_i N_1$. If any other external forces do not act on the pendulum, then under the action of such a moment it rotates with constant angular velocity. If the system is in a gravitational field (g=9.81[m/s^2] - acceleration of gravity), the weight of the pendulum causes the unevenness of its rotation: the pendulum slows down, when the center of mass rises up and accelerates when the center of mass falls down. It is assumed that N_1>0.0. If N_{0i} torque is positive, the pendulum rotates to the left having a positive value of the instantaneous angular velocity, if N_{0i}<0.0, the pendulum rotates to the right with a negative angular velocity.

The equations of motion described above are as follows:

$$B\,\ddot{\varphi}_i + m\ddot{x}l\cos\varphi_i + c_\varphi\dot{\varphi}_i + mgl\sin\varphi_i = N_{0i} - \dot{\varphi}_i N_1, \tag{1}$$

$$(M+nm)\ddot{x} + c_x\dot{x} + k_x x = \sum_{i=1}^{n} m\,l\left(-\ddot{\varphi}_i\cos\varphi_i + \dot{\varphi}_i^2\sin\varphi_i\right), \tag{2}$$

where i=1,2,…n. In our numerical simulations eqs.(1,2) have been integrated by the 4th order Runge-Kutta method. The obtained results confirmed the existence of the phenomenon of phase synchronization in the considered system and allowed the determination of phase angles between the synchronized pendula. Additionally the numerical integration of eqs.(1,2) allows the determination of the basins of attraction of different coexisting configurations of the synchronized pendula. We use the following parameters' values: m=1.00 [kg], l=0.25 [m], c_φ=0.01 [Nsm], N_1=0.50 [Nsm], M=6.00 [kg]. It has been considered that pendulum 1 rotates counterclockwise and pendula 2,…n clockwise so N_{01}=5.00 [Nm], N_{0i}=-5.00 [Nm] (i=2,…,n). We assume that at the initial state: x_0=0.0, $\dot{x}_0 = 0$ (the beam is at rest) and the pendula are

rotating in opposite directions with equal velocities $\dot{\varphi}_{10} = \omega_1 = 10.0\,[\mathrm{s}^{-1}]$, $\dot{\varphi}_{i0} = \omega_i = -10.0\,[\mathrm{s}^{-1}]$, i=2,…,n. Other initial conditions are given by the pendula's initial positions φ_{i0}.

3. Synchronization condition - linearized model

In this section we derive the approximate analytical conditions for synchronization of rotating pendula. Following the idea of Blekhman [4] to explain the phenomena of synchronization we determine and analyze the work done by the momentum with which the i-th pendulum acts on beam - W_i^{SYN}.

In our analysis we assume that the system consists of three identical pendula. This assumption allows the derivation of the approximate analytical result which explains the synchronization of two and three pendula and can be generalized for larger number of pendula. It also justifies the existence of clusters (groups of pendula with identical behavior. We assume that the pendula's angular velocities are constant, i.e., the fluctuations of the pendula's angular velocities caused by the motion in the gravitational field are so small that can be neglected. Hence, the pendula's accelerations are equal to zero and one gets linear functions describing the pendula's angles of rotation:

$$\begin{aligned}
&\dot{\varphi}_1 = \omega,\\
&\dot{\varphi}_2 = \dot{\varphi}_3 = -\omega,\\
&\varphi_1 = \omega t + \beta_1,\\
&\varphi_2 = -\omega t + \beta_2,\\
&\varphi_3 = -\omega t + \beta_3,\\
&\ddot{\varphi}_1 = \ddot{\varphi}_2 = \ddot{\varphi}_3 = 0.0.
\end{aligned} \tag{3}$$

The right side of equation (2) shows the resultant force, which acts on the beam:

$$\begin{aligned}
&F = \sum_{i=1}^{3} ml\left(-\ddot{\varphi}_i \cos\varphi_i + \dot{\varphi}_i^2 \sin\varphi_i\right) =\\
&= lm\omega^2\left(\sin(\omega t + \beta_1) + \sin(-\omega t + \beta_2) + \sin(-\omega t + \beta_2)\right).
\end{aligned} \tag{4}$$

After the transformation:

$$\begin{aligned}
&F = \omega^2 ml(\sin\omega t\cos\beta_1 + \cos\omega t\sin\beta_1) +\\
&+ \omega^2 ml(-\sin\omega t\cos\beta_2 + \cos\omega t\sin\beta_2) +\\
&+ \omega^2 ml(-\sin\omega t\cos\beta_3 + \cos\omega t\sin\beta_3)
\end{aligned} \tag{5}$$

Substituting eq. (5) to the equations of motion of the beam (2) and denoting

$$U = M + nm, \tag{6}$$

one gets

$$\begin{aligned}
&U\ddot{x} + c_x\dot{x} + k_x x = \omega^2 ml(\sin\omega t\cos\beta_1 + \cos\omega t\sin\beta_1) +\\
&+ \omega^2 ml(-\sin\omega t\cos\beta_2 + \cos\omega_2 t\sin\beta_2) + \omega^2 ml(-\sin\omega t\cos\beta_3 + \cos\omega_2 t\sin\beta_3).
\end{aligned} \tag{7}$$

Assuming that the damping coefficient c_x is small the functions describing the displacement and acceleration of the beam can be rewritten as

$$\begin{aligned}
&x = X_1 ml(\sin\omega t\cos\beta_1 + \cos\omega t\sin\beta_1) + X_1 ml(-\sin\omega t\cos\beta_2 + \cos\omega_2 t\sin\beta_2) +\\
&+ X_1 ml(-\sin\omega t\cos\beta_3 + \cos\omega t\sin\beta_3)
\end{aligned} \tag{8}$$

$$\begin{aligned}
&\ddot{x} = A_1 ml(\sin\omega t\cos\beta_1 + \cos\omega t\sin\beta_1) + A_1 ml(-\sin\omega t\cos\beta_2 + \cos\omega_2 t\sin\beta_2) +\\
&+ A_1 ml(-\sin\omega t\cos\beta_3 + \cos\omega_2 t\sin\beta_3)
\end{aligned} \tag{9}$$

where

$$X_1 = \frac{\omega^2}{k_x - \omega^2 U}, A_1 = \frac{-\omega^4}{k_x - \omega^2 U} \tag{10}$$

The equation of motion of each pendulum (1) has a component

$$M_k^{SYN} = ml\ddot{x}\cos\varphi_k. \tag{11}$$

that is called the synchronizing momentum. This is the momentum of the force with which the beam acts on the *k*-th pendulum. The work done by this torque increases or decreases the energy of the *k*-th pendulum. In the synchronous state pendula's motion is periodic so the work done by these momenta during one period of rotation is equal to zero:

$$W_k^{SYN} = \int_0^T (ml\ddot{x}\cos\varphi_k)\dot{\varphi}_k dt = 0. \tag{12}$$

Substituting eqs. (3) and (9) into eq. (12) one gets

$$\begin{aligned}
W_1^{SYN} &= l^2 A_1 \omega m^2 \int_0^T \begin{bmatrix} [\sin\omega t\cos\beta_1 + \cos\omega t\sin\beta_1] + \\ +[-\sin\omega t\cos\beta_2 + \cos\omega t\sin\beta_2] + \\ +[-\sin\omega t\cos\beta_3 + \cos\omega t\sin\beta_3] \end{bmatrix} (\cos\omega t\cos\beta_1 - \sin\omega t\sin\beta_1)dt = 0, \\
W_2^{SYN} &= l^2 A_1 (-\omega) m^2 \int_0^T \begin{bmatrix} [\sin\omega t\cos\beta_1 + \cos\omega t\sin\beta_1] + \\ +[-\sin\omega t\cos\beta_2 + \cos\omega t\sin\beta_2] + \\ +[-\sin\omega t\cos\beta_3 + \cos\omega t\sin\beta_3] \end{bmatrix} (\cos\omega t\cos\beta_2 + \sin\omega t\sin\beta_2)dt = 0, \\
W_3^{SYN} &= l^2 A_1 (-\omega) m^2 \int_0^T \begin{bmatrix} [\sin\omega t\cos\beta_1 + \cos\omega t\sin\beta_1] + \\ +[-\sin\omega t\cos\beta_2 + \cos\omega t\sin\beta_2] + \\ +[-\sin\omega t\cos\beta_3 + \cos\omega t\sin\beta_3] \end{bmatrix} (\cos\omega t\cos\beta_3 + \sin\omega t\sin\beta_3)dt = 0.
\end{aligned} \tag{13}$$

After the transformation the following equations can be obtained

$$\begin{aligned}
W_1^{SYN} &= l^2 A_1 \omega m^2 \pi\big(m_1 m_1 \sin(\beta_1 - \beta_1) + m_1 m_2 \sin(\beta_1 + \beta_2) + m_1 m_3 \sin(\beta_1 + \beta_3)\big) = 0 \\
W_2^{SYN} &= l^2 A_1 \omega m^2 \pi\big(-m_1 m_2 \sin(\beta_1 + \beta_2) + m_2 m_2 \sin(\beta_2 - \beta_2) + m_2 m_3 \sin(\beta_2 - \beta_3)\big) = 0 \\
W_3^{SYN} &= m^2 l^2 A_1 \omega m^2 \pi\big(-m_3 m_1 \sin(\beta_1 + \beta_3) + m_3 m_2 \sin(\beta_3 - \beta_2) + m_3 m_3 \sin(\beta_3 - \beta_3)\big) = 0
\end{aligned} \tag{14}$$

Eqs.(14) allow the calculation of the value of phase angles β_i at which the motion of pendulums synchronization occurs, and thus the motion of the system is periodic.

In the case of n=2 pendula, i.e., assuming that m_3=0 and β_1=0.0 eqs.(14) get the form of two identical equations:

$$\begin{aligned}
\sin(\beta_2) &= 0 \\
\sin(\beta_2) &= 0
\end{aligned} \tag{15}$$

which are fulfilled in two cases: (i) β_2=0.0^o - the *mirror-synchronization* (*M*) shown in Figure 2(b), (ii) β_2=180.0^o - the *antiphase synchronization* (*A*) shown in Figure 2(d).

For three pendula, i.e., assuming that β_1=0.0, eqs.(14) get the following form:

$$\begin{aligned}
&\sin(\beta_2) + \sin(\beta_3) = 0 \\
&\sin(\beta_2) - \sin(\beta_2 - \beta_3) = 0 \\
&\sin(\beta_3) - \sin(\beta_3 - \beta_2) = 0
\end{aligned} \tag{16}$$

and eqs.(16) are fulfilled for: (i) β_2=-60.0^o and β_3=-300.0^o - the *tree-synchronization* (*T*) shown in Figure 4(a), (ii) β_2=β_3= 180.0^o – the *cluster-antiphase synchronization* (*CA*) shown in Figure 4(b).

4. Examples

4.1 Synchronization of 2 and 3 pendula (the lack of gravity)

In order to confirm the analytical results of Sec. 3 we perform the numerical simulations of eqs.(1,2). Stiffness coefficient k_x has been taken as a control parameter in such a way that the base is above or below the resonance, i.e., to the frequency

$$\alpha_x = \sqrt{\frac{k_x}{U}}. \tag{17}$$

is smaller or larger than the pendulum's 1 angular velocity ω_1. The damping coefficient c_x has been selected in such a way as to be equivalent to the arbitrarily selected logarithmic decrement of damping $\Delta=\ln(1.5)$. As such a damping does not significantly change the period of the beam's free oscillations c_x can b calculated from the formula

$$c_x = \frac{\Delta\sqrt{k_x U}}{\pi}. \tag{18}$$

The value of the parameter g in eqs. (1) is equal to zero - this can be interpreted as the case in which the pendula are rotating in the horizontal plane. The results obtained for the system with two pendula are shown in Figure 2(a-d). Figure 2(a) shows the time series of the pendula's angular velocities $\dot{\varphi}_1$ and $\dot{\varphi}_2$ for the small value of the stiffness coefficient k_x=500.0 [N/m] (so $\alpha_x=(500.0/8.0)^{0.5}=7.91<10.0=\omega_1$ and the system is below the resonace). On the horizontal axis time is given by $K=\omega_1 t/2\pi$, i.e., the number of rotations of the pendulum 1 (rotating with the angular velocity ω_1). In our calculations we use the following initial conditions: $\varphi_{10}=0.0^o$, $\varphi_{20}=-90.0^o$. As one can see, after a short (several rotations) transient caused by the motion of the beam, pendula's angular velocities tend to their initial values ω_1 and ω_2. Figure 2(b) shows the sum of pendula's angular displacements $\varphi_2+\varphi_1$. As one can see this sum (after the transitional period) is constant and equal to zero, which means that $\varphi_2=-\varphi_1$. This state is the *mirror-synchronization* (*M*) as the rotational motion of pendulum 2 is a mirror image of the rotation motion of pendulum 1 and the beam is at rest as shown in Figure 2(b). The pendula pass each other as going through the vertical plane of symmetry ($\varphi_1=0.0^o \Rightarrow \varphi_2=0.0^o$ or $\varphi_1=180.0^o \Rightarrow \varphi_2=-180.0^o$). For the same value of the stiffness coefficient but different initial conditions one can observe a different type of synchronization. For example for: $\varphi_{10}=0.0^o$, $\varphi_{20}=-215.0^o$, after a transient the sum of pendula's displacements $\varphi_2+\varphi_1$ reaches the value $\varphi_2+\varphi_1=-180^o$ as shown in Figure 2(d). The pendula's velocities (Figure 2(c)) fluctuate around the averaged values smaller (by absolute values) than initial values ω_1 and ω_2. These fluctuations are caused by the oscillations of the beam. This type of synchronization is the *antiphase-synchronization* (*A*). The pendula pass each other as going through the horizontal plane of symmetry ($\varphi_1=90.0^o \Rightarrow \varphi_2=-270.0^o$ or $\varphi_1=270.0^o \Rightarrow \varphi_2=-90.0^o$.

The influence of the stiffness coefficient k_x and initial position of the pendulum 2 - φ_{20} on the type of synchronization is illustrated in Figure 3 (initial position of pendulum 1 – $\varphi_{10}=0^o$). One can see that for the small values of the stiffness coefficient $k_x<453.0$ [N/m] for all values of φ_{20} the mirror-synchronization occurs. In the interval $453.0<k_x<758.0$ [N/m] depending on the initial condition φ_{20} either mirror- or antiphase- synchronization occurs. For $k_x>758$ [N/m] and any value of φ_{20} we observe the antiphase-synchronization.

Figure 4(a) presents the sums of pendula's displacements $\varphi_2+\varphi_1$, $\varphi_3+\varphi_1$ for the small stiffness coefficient k_x=200.0 [N/m] ($\alpha_x=(200.0/9.0)^{0.5}=4.71<10.0=\omega_1$). The following initial

conditions have been used: φ_{10}=0.0°, φ_{20}=-60.0°, φ_{30}=-240.0°. One can see that after the initial transient the sum $\varphi_2+\varphi_1$ reaches the constant value -60° and the sum $\varphi_3+\varphi_1$ reaches the constant value -300°. This type of synchronization (shown at the diagram in Figure 4(a) for φ_1=0.0°) is the *tree-synchronization* (*T*) (for different initial conditions one observes symmetrical configuration in which pendula 2 and 3 are respectively in the right and in the left hand sides of the diagram). Increasing the value of the stiffness coefficient to k_x=1000.0 [N/m] (α_x=(1000.0/9.0)$^{0.5}$= =10.54>10.0=ω_1, i.e., the beam is above the resonance) and changing the pendula's initial position to φ_{10}=0.0°, φ_{20}=-180.0°, φ_{30}=-90.0° (other initial conditions are as in the case shown in Figure 4(a)) one gets the synchronous state in which pendula 2 and 3 (rotating to the left) create the cluster (their displacements are the same) – Figure 4(b). The sum of displacements of any pendulum in cluster and pendulum 1 - $\varphi_2+\varphi_1=\varphi_3+\varphi_1$ reaches the value 180°, which justifies the name *cluster-antiphase-synchronization* (*CA*). The pendula's configuration during this type of synchronization is shown at the diagram in Figure 4(b) (for φ_{10}=0.0°). Figure 4(c) shows the basins of existance of both types of synchronization at the plane k_x-φ_{30}. We consider φ_{10}=0.0°, φ_{20}=-135° and other initial conditions as in Figure 4(a). For k_x<330 [N/m] and all initial conditions we observe (*T*) synchronization. In the interval 330<k_x<460 [N/m] the type of synchronization depends on initial conditions. For k_x>460 [N/m] independently of the initial conditions the system reaches (*CA*) synchronization.

4.2 Synchronization of two pendula (in the gravitational field)

In the simulations shown in Figure 5(a-d) we consider the system of two pendula rotating in the vertical plane, i.e., considering the effect of gravity (*g*=9.81 [m/s^2]). Figure 5(a) presents time series of the pendula's angular velocities $\dot{\varphi}_1$ and $\dot{\varphi}_2$ for the small value of the stiffness coefficient k_x=500.0 [N/m], so α_x=(500.0/8.0)$^{0.5}$=7.91<10.0=ω_1. The pendula rotate in opposite directions with constant velocities $\dot{\varphi}_{10}=\omega_1=10.0\,[s^{-1}], \dot{\varphi}_{20}=\omega_2=-10.0\,[s^{-1}]$ starting from the initial positions: φ_{10}=0.0°, φ_{20}=-45.0°. One can see that after the initial transient (several rotations) caused by the oscillations of the beam the pendula's velocities fluctuate (due to the gravity) around the initial values ω_1 and ω_2. Figure 5(b) shows time series of the sum of pendula's displacements $\varphi_2+\varphi_1$. One can see that this sum (after the initial transient) is constant and equal to zero so $\varphi_2=-\varphi_1$. This type of synchronization is the *mirror-synchronization* (*M*) as the rotational motion of pendulum 2 is the mirror image of the rotations of pendulum 1 as can be seen at the diagram shown in Figure 5(b). For the small value of the stiffness coefficient k_x=500.0 [N/m] and different initial conditions φ_{10}=0.0°, φ_{20}=-215.0° one can observe different type of synchronization as shown in Figure 5(c,d). After the initial transient the pendula's velocities (as in the previous case) fluctuate around the initial values ω_1 and ω_2 (Figure 5(c)). The sum of pendula's displacements $\varphi_2+\varphi_1$ fluctuates around the constant averaged value $<\varphi_2+\varphi_1>=-180°$ as shown in Figure 5(d). We call this type of synchronization the *antiphase-synchronization* (*A*). For the larger values of k_x the next type of synchronization can be observed. Figure 6(a,b) illustrates pendula's synchronization for large values of the stiffness coefficient k_x=3000.0 [N/m] and α_x=(3000.0/8.0)$^{0.5}$=19.36>10.0=ω_1. We consider the following initial conditions: φ_{10}=0.0°, φ_{20}=-270.0°. After the initial transient the sum of pendula's displacements $\varphi_2+\varphi_1$ fluctuates around constant averaged value $<\varphi_2+\varphi_1>$ close to -270° as shown in Figure 6(a). We call this type of synchronization the *third-quarter-synchronization* (*3Q*). When pendulum 1 passes

through the static equilibrium position pendulum 2 approaches the horizontal plane of symmetry ($\varphi_1 = 0.0^o \Rightarrow \varphi_2 \approx -270.0^o$).

For different initial conditions: $\varphi_{10}=0.0^o$, $\varphi_{20}=-90.0^o$, after the initial transient the sum of pendula's displacements $\varphi_2 + \varphi_1$ fluctuates around constant averaged value $<\varphi_2 + \varphi_1>$ closed to -90^o as shown in Figure 6(b). This type of synchronization has been called the *first-quarter-synchronization* (*1Q*). When pendulum 1 passes through the static equilibrium position pendulum 2 leaves the horizontal plane of symmetry ($\varphi_1 = 0.0^o \Rightarrow \varphi_2 \approx -90.0^o$). The pendula's configurations during (1Q) and (3Q) synchronizations are shown at diagrams in Figure 6(a,b). (*3Q*) and (*1Q*) synchronizations are not observed when one neglects the effect of gravity or when the pendula rotate in the horizontal plane. In both cases the pendula's velocities oscillate around the initial values ω_1 and ω_2 as in the examples shown in Figure 5(a,c).

The influence of the stiffness coefficient k_x and initial conditions on the type of synchronization is discussed in Figure 7(a-d). Figure 7(a) presents the averaged value of the sum of pendula's displacements $<\varphi_2+\varphi_1>$ versus stiffness coefficient k_x. For all values of k_x the motion of the system is initiated from the same initial conditions. In Figure 7(a) we show the averaged value of the sum of pendula's displacements $<\varphi_2+\varphi_1>$ versus the stiffness coefficient k_x for the following initial conditions: $\varphi_{10}=0.0^o$, $\varphi_{20}=-270.0^o$. One can see that for the small values of the stiffness coefficient $k_x<360.0$ [N/m], the value of $<\varphi_2+\varphi_1>=0^o$ and the system is in the state of mirror-synchronizaton (*M*). For $k_x=360.0$ [N/m] the value of $<\varphi_2+\varphi_1>$ jumps to -180^o and in the interval $360.0<k_x<1910.0$ [N/m] we observe antiphase-synchronization (*A*). For $k_x=1910.0$ [N/m] the next jump of $<\varphi_2+\varphi_1>$ (to the value of -240^o) occurs and the type of synchronization is changed to the third-quarter-synchronization (*3Q*). In the interval $1910.0<k_x<5000.0$ [N/m] in the state of the third-quarter-synchronization (*3Q*) the value of $<\varphi_2+\varphi_1>$ initially decreases down to the value -254^o and later increases up to the value -180^o, so we observe the return to the state of antiphase-synchronization (*A*). Figure 7(b) shows the value of $<\varphi_2+\varphi_1>$ versus k_x for different initial conditions (we change the value of φ_{20} from $\varphi_{20}=-270.0^o$ to $\varphi_{20}=-270.0^o$). As in Figure 7(a) for small values of k_x first we observe the state of the mirror-synchronizaton (*M*) and next the antiphase-synchronization (*A*). The jump of the value of $<\varphi_2+\varphi_1>$ to -118^o, observed for $k_x=1960.0$ [N/m], indicates the change of the type of synchronization to the first-quarter (*1Q*). In the interval $1960.0<k_x<5000.0$ [N/m] in the state of the first-quarter-synchronization, the value of $<\varphi_2+\varphi_1>$ initially increases up to -104^o and next decreases down to -180^o, so we observe the return to the state of antiphase-synchronization (A). Figure 7(c) presents the influence of the initial conditions φ_{10} and φ_{20} on the type of synchronization for the small value $k_x=500.0$ [N/m] (types (*M*) and (*A*) are observed) while Figure 7(d) shows basins of (*3Q*) and (*1Q*) for large value of $k_x=3000.0$ [N/m].

The influence of the stiffness coefficient k_x and initial position of pendulum 2 - φ_{20} on the type of synchronization is discussed in Figure 8. We assume the initial position of the pendulum 1 - $\varphi_{10}=0^o$. One can see that for small values of the stiffness coefficient $k_x<425.0$ [N/m] and any value of φ_{20} the mirror-synchronization (*M*) occurs. In the interval $425.0<k_x<760.0$ [N/m], depending on initial condition φ_{20} one observes mirror (*M*) or antiphase (*A*) synchronization. (*A*) and (*M*) types of synchronization observed for $k_x=500.0$ [N/m] are shown in Figure 7(c). In the interval $760.0<k_x<1960.0$ [N/m] for any value of φ_{20} antiphase-synchronization (*A*) occurs. For $k_x>1960.0$ [N/m] depending on initial condition φ_{20} we observe the third-quarter (*3Q*) or the first-quarter (*1Q*) synchronization. (1Q) and (3Q) types of synchronization observed for $k_x=3000.0$ [N/m] are shown in Figure 7(d).

4.3. Synchronization of three pendula (in the gravitational field)

In the simulations of the system of three pendula rotating in the vertical plane, i.e., considering the effect of gravity, we use the same parameter values as in example 4.2 and additionally consider N_{03}=-5.00 [Nm], i.e., pendulum 1 rotates counterclockwise and pendula 2 and 3 clockwise.

Figure 9(a-d) shows time series of the sum of pendula's displacements $\varphi_2+\varphi_1$ and $\varphi_3+\varphi_1$ during four different synchronous states. In Figure 9(a) we present time series for the case of small stiffness coefficient k_x=200.0 [N/m], so α_x=(200.0/9.0)$^{0.5}$=4.71<10.0=ω and the following initial conditions: φ_{10}=0.0^o, φ_{20}=-60.0^o, φ_{30}=-240.0^o. After the initial transient the sum of pendula's displacements $\varphi_2+\varphi_1$ fluctuates around constant averaged value approximately equal to -60^o, and the sum $\varphi_3+\varphi_1$, fluctuates around the averaged value close to -300^o. This type of synchronization we call the tree synchronization (*T*). The pendula's configuration for φ_1=0.0^o is shown at the diagram in Figure 9(a). Increasing the value of the stiffness coefficient to k_x=1000.0 [N/m] (so α_x=(1000.0/9.0)$^{0.5}$= 10.54>10.0=ω and the beam oscillations are above the resonance) and changing the initial positions of the pendula to φ_{10}=0.0^o, φ_{20}=-180.0^o, φ_{30}=-90.0^o (other initial conditions are the same as in Figure 9(a) one observes the synchronous state in which pendula 2 and 3 (rotating to the left) create the cluster (their displacements are identical) as shown in Figure 9(b).The sum of the displacements of any pendulum in cluster and pendulum 1 $\varphi_2+\varphi_1=\varphi_3+\varphi_1$ fluctuates around constant average value $<\varphi_2+\varphi_1>=<\varphi_3+\varphi_1>$ approximately equal to -180^o and we observe the cluster-antiphase-synchronization (*CA*). The pendula's configuration during this type of synchronization for φ_1=0.0^o is shown at the diagram in Figure 9(b). Additionally in the system with three pendula one can observe four new types of synchronization which occur due to the existence of gravity and the change of the amplitude and phase of the beam's oscillations (as the result of the increased value of the stiffness coefficient k_x). For k_x=3000.0 [N/m] and initial conditions φ_{10}=0.0^o, φ_{20}=-250.0^o, φ_{30}=-80.0^o, we observe the type of synchronization similar to (*T*) synchronization but with obtuse angles between pendulum 1 and pendula 2,3 as shown at the diagram in Figure 9(c). We call this synchronization the *yankee 32* (*Y32*) - synchronization. For different initial conditions one can observe the pendula's configuration which is the mirror image of (*Y32*), i.e., pendulum 3 is on the right side and pendulum 2 on the left side of the diagram. This configuration is called the *yankee 23* (*Y23*) – synchronization. For the same value of the stiffness coefficient k_x and initial conditions: φ_{10}=0.0^o, φ_{20}=-250.0^o, φ_{30}=-180.0^o we observe the type of synchronization shown in Figure 9(d). This synchronization is similar to (*CA*) synchronization, but the angle between the cluster (of pendula 2 and 3) and pendulum 1 is approximately equal to -270^o (the *cluster-right*-synchronization (*CR*)) or -90^o (the *cluster-left*-synchronization (*CL*)).

Figure 10(a-d) shows the influence of stiffness coefficient k_x on the type of the synchronous state. The averaged values of the sums of pendula's displacements $<\varphi_2+\varphi_1>$ and $<\varphi_3+\varphi_1>$ versus k_x are shown. For all values of k_x the motion of the system is initiated from the same initial conditions. In the system with small stiffness coefficient k_x one observes (*T*) type synchronization as can be seen in Figure 10(a-d). For larger values of k_x we observe (*CA*) synchronization and finally for k_x>2200÷2400 [N/m] (exact value depends on φ_{30}) two other types of synchronization (*CR*) and (*Y32*) and their mirror images (*CL*) and (*Y23*) are possible.

Figure 10(a-d) shows that the values $<\varphi_2+\varphi_1>$ and $<\varphi_3+\varphi_1>$ are changing with the change of k_x, so the descriptions of the pendula's configurations in different types of synchronizations with the statements about the angles close to 180^o in the case of (*CA*) or 270^o and 90^o in the case of (*CR*) and (*CL*) present only the qualitative differences. Particularly in Figure 10(c) the distinction between (*CA*) and (*CL*) synchronization is arbitrary, due to the continuous change of the angle between cluster (pendula 2 and 3) and pendulum 1. In the other cases the distinction between different types of synchronization is justified by the jump changes of angles $<\varphi_2+\varphi_1>$ and (or) $<\varphi_3+\varphi_1>$. The cross sections shown in Figure 10(a-d) are indicated in Figure 11(a). Figure 11(a) shows the basins of existence of different types of synchronization on the plane k_x-φ_{30}. We consider the following initial conditions $\varphi_{10}=0.0^o$, $\varphi_{20}=-135^o$. Figure 11(b) shows the enlargement of Figure 11(a) for $200<k_x<400$ [N/m]. From Figure 11(a,b) one can conclude that for stiffness coefficient $k_x<2200\div2400$ [N/m] one can observe either (*T*) ($k_x<300\div370$ [N/m]) or (*CA*) synchronization ($300\div370<k_x<2200\div2400$ [N/m]). The type of synchronization depends on the value of k_x only in the neighborhood of the boundaries between basins (*T*) and (*CA*) as shown in 11(b) and 11(d). Figure 11(d) presents the cross section of Figure 11(b) on level $k_x=325$ [N/m] which shows the coexistence of (*T*) and (*CA*) synchronizations for different initial conditions φ_{20} and φ_{30}. For larger values of k_x we observe the coexistence of four types of synchronization as can be seen in Figure 11(a,c). Figure 11(c) is the cross section of Figure 11(a) at level $k_x=3000$ [N/m].

4.4 Larger systems

In an attempt to generalize the results of Secs. 4.1-4.3 to the system with larger number of pendula we perform simulations of such systems. Figure 12(a,b) shows results obtained for the case in which pendula oscillate in the horizontal plane (i.e., $g=0.0$). In Figure 12(a) we show the time series of the sum of pendula's displacements $\varphi_i+\varphi_1$ ($i=2\ldots6$) for the small stiffness coefficient $k_x=200.0$ [N/m]. The following initial conditions have been used: $\varphi_{10}=0.0^o$, $\varphi_{20}=-5.0^o$, $\varphi_{30}=-10.0^o$, $\varphi_{40}=-15.0^o$, $\varphi_{50}=-20.0^o$, $\varphi_{60}=-25.0^o$. After the short transient (several rotations) the sums of pendula's displacements tends to the constant values close to 0^o, $\pm90^o$ and $\pm120^o$ (the exact values can be calculated from the equations equivalent to eqs. (16). Observed synchronization is analog to the tree-synchronization (*T*) described for the system with three pendula. Similar configurations in which the pendula are not grouped in clusters have been observed in the systems with larger number of pendula. Figure 12(b) shows that the increase of the stiffness coefficient to $k_x=2000.0$ [N/m] leads to the change of the synchronization type to cluster-antiphase-synchronization (*CA*). Neglecting the influence of gravity we obtain this type of synchronization independently of initial conditions for sufficiently large values of k_x .

Figure 13(a-d) shows examples of pendula's configurations for the system in which pendula rotate in the vertical plane (i.e., $g=9.81$ [m/s^2] in eqs.(1-2)). In Figure 13(a) we show the sums of pendula's displacements $\varphi_i+\varphi_1$ ($i=2\ldots6$) for the system with small stiffness $k_x=200.0$ [N/m]. The same initial condition as in the example of Figure 12(a) have been used. One can see that after the initial transient (several rotations) the sums of pendula's displacements fluctuate around constant values close to these observed in Figure 12(a), i.e., 0^o, $\pm90^o$ and $\pm120^o$. This type of synchronization is equivalent to the tree-synchronization (*T*). Figure 13(b) presents that the increase of the stiffness coefficient to $k_x=2000.0$ [N/m] leads to the change of the type of synchronization to the cluster-antiphase (*CA*) (similarly to the case shown in Figure 12(b)). Figure 13(c,d) shows that with further increase of the stiffness coefficient, e.g. to the value $k_x=3000.0$ [N/m] the type of synchronization depends on the

initial conditions as one can observe either (*CL*) (Figure 13(c)) or *Yankee* (Figure 13(d)) synchronization.

Generally in the systems with large number of pendula we observe the same types of synchronizations as described for three pendula in Secs. 4.1 and 4.3. Probability of the appearance of the yankee type of synchronization decreases with the increase of the number of pendula.

5. Conclusions

In the system in which the pendula rotate in opposite directions one can observe different types of synchronization. During the synchronous motion the average (over the period of rotation) value of the sum of angular displacements of pendula rotating to the right and left is constant. Our approximate analytical studies of synchronization momenta, i.e., momenta responsible for energy transfer between pendula, allow prediction of the mirror (*M*), antiphase (*A*) synchronization in the system of n=2 pendula and tree (*T*) and cluster antiphase (*CA*) synchronization in the system of n=3 pendula. These types of synchronization occur for both horizontal (without gravity) and vertical (in the gravitational field) planes of pendula rotation.

Numerical simulations confirm the existence of these types of synchronization. In the system with two pendula they additionally show that due to gravity, at sufficiently large values of the stiffness coefficient of stiffness k_x, one can observe two modifications of the (*A*) type synchronization, namely the first-quarter (*1Q*) and the third-quarter (*3Q*) synchronization. In the system with three pendula we show that the analytically predicted tree (*T*) and cluster antiphase (*CA*) types of synchronization occur independently of the consideration of gravity. For pendula rotation in the gravitational field one can also observe, for sufficiently large values of the stiffness coefficient k_x, two modifications of the (*T*) type, i.e., yankee (*Y23*) and yankee (*Y32*) synchronization and two modifications (*CA*) type: (*CL*) and (*CR*) synchronization. The types of synchronization which have been observed for the sysyems with two and three pendula together with the conditions for their occurrence are summarized in Table 1.

The types of synchronous configurations identified for the system of three pendula can be observed in the systems with larger number of pendula. Contrary to the case of oscillating pendulums [21,22] rotating pendula are not grouped in three or five clusters only. The lack of this restriction causes that in the system (1,2) depending on initial condition one can observe a great variety of different synchronization configurations. The number of configurations grows with a number of pendulums n.

The system with identical pendula which rotate with the same (as to the absolute values) angular velocities located on the beam *M* which can oscillate horizontally (i.e., $k_x<\infty$) always reaches the state of synchronization. In the case of the non-movable beam *M* ($k_x=\infty$) when the pendula cannot interact as their velocities have the same absolute values and constant phase differences between pendula are constant and defined by the initial conditions. When the oscillations of the beam *M* allow the interaction between pendula the process of synchronization is initiated and the phase differences between pendula's rotations tends to some characteristic values, e.g.: 0, 180^o, 270^o, etc. (in the case of pendula rotating in the horizontal plane) or oscillate around these values (in the case of pendula rotating in the vertical plane).

The lack of synchronization, i.e., a state in which such $\varphi_1+\varphi_2$ is not constant or periodic (when pendula rotate in horizontal plane) is observed in certain ranges of parameters in the system of pendula with different masses which rotate with different angular velocities but the results of these studies will be report elsewhere [23].

Practical applications of the devices with rotating links (pendulums) can be divided into two classes: (i) devices in which the large oscillations of the pendula's base are desired, e.g.: shakers, mixers, sieve, etc., and (ii) devises in which the large oscillations of the pendulums' base are not desired, e.g., several machines with unbalanced links located on the flexible ceiling. Our results can be useful for the designers of the devises with rotational links as they show what types of synchronization can be expect and allow estimation of the impact on the pendula's rotation on the base.

Acknowledgment: This work has been supported by the Polish Department for Scientific Research (DBN) under project No. N N501 249238 and partially by the Foundation for Polish Science, Team Programme – Project No. TEAM/2010/5/5

References

1. Lee, C.W. Vibration Analysis of Rotors, (Kluwer, New York, 1993).
2. Czolczynski, K. Rotordynamics of Gas-Lubricated Journal Bearing Systems, (Springer, New York, 1999).
3. Vance, J.M., Fouad Y. Zeidan, F.,Y., Murphy, B. Machinery Vibration and Rotordynamics, (Wiley, London, 2010).
4. Blekhman I.I. Synchronization in Science and Technology, (ASME Press, New York, 1988).
5. Balthazar, J.M., Palacios Felix, J.L., and Brasil, R.,MLRF, **[**2005]. Some comments on the numerical simulation of self-synchronization of four non-ideal exciters. Applied Mathematics and Computation 2005; 164, 615–625.
6. Boccaletti, S., Kurths, J., Osipov, G., Valladares, D. L. & Zhou, C. S. The synchronization of chaotic systems, Phys. Rep. 2002: 366, 1-101.
7. Rosenblum, M.G., Pikovsky, A.S., and Kurths, J. Phase synchronization of chaotic oscillators. Physical Review Letters. 1996: 76, 1804-1807
8. Rosenblum, M.G., Pikovsky, A.S., and Kurths, J. From phase to lag synchronization in coupled oscilators. Physical Review Letters. 1997: 78, 4193-4196.
9. Fillipov, A., Hu, B., Li, B. and Zeltser,A. Energy transport between two attractors connected by a Fermi-Pasta-Ulam chain, J. Phys. A: Math. Gen. 1998: 31, 7719.
10. Prasad**, A.,** Universal occurrence of mixed-synchronization in counter-rotating nonlinear coupled oscillators, Chaos, Solitons and Fractals 2010: 43, 42-46.
11. Wiercigroch, M. A new concept of energy extraction from waves via parametric pendulor, Personal Communications, 2003.
12. Xu, X., Wiercigroch M. and Cartmell, M.P. Rotating orbits of a parametrically-excited pendulum, Chaos, Solitons and Fractals 2005: 23(5), 1537-1548.
13. Xu, X. Nonlinear dynamics of parametric pendulum for wave energy extraction, PhD Thesis, Aberdeen University, 2005.
14. Xu, X. and Wiercigroch, M. Approximate analytical solutions for oscillatory and rotational motion of a parametric pendulum", Nonlinear Dynamics 2007: 47, 311-320.
15. Xu, X., Pavlovskaia E., Wiercigroch, M., Romeo, F. and Lenci, S. Dynamic interactions between parametric pendulum and electro-dynamical shaker, ZAMM 2007: 87(2), pp. 172-186.
16. Lenci S. and Rega G. Competing dynamic solutions in a parametrically excited pendulum: attractor robustness and basin integrity, ASME J. Comp. Nonlin. Dyn., 2008: 3(4), 41010.

17. Lenci, S., Pavlovskaia, E., Rega, G. and Wiercigroch, M. Rotating solutions and stability of parametric pendulum by perturbation method", Journal of Sound and Vibration 2008: 310, 243-259.
18. Horton, B. Rotational motion of pendula systems for wave energy extraction, PhD Thesis, Aberdeen University, 2008.
19. Thompson, J. M. T., Wiercigroch, M., Sieber, J. and Horton, B. W. Dynamics of the nearly parametric pendulum. International Journal of Non-Linear Mechanics, 2011: 46, 436-442
20. Czolczynski, K., Perlikowski, P. Stefanski, A., and Kapitaniak, T. Synchronization of slowly rotating pendulums, Int. J. Bifur. Chaos., (in press)
21. Czolczynski, K., Perlikowski, P. Stefanski, A., and Kapitaniak, T. Clustering of Huygens' Clocks, Progress of Theoretical Physics, 2009: 122, 1027-1033.
22. Czolczynski, K., Perlikowski, P. Stefanski, A., and Kapitaniak, T. Clustering and Synchronization of Huygens' Clocks". Physica A, 2009: 388, 5013-5023.
23. Czolczynski, K., Perlikowski, P. Stefanski, A., and Kapitaniak, T. (*in preparation*)

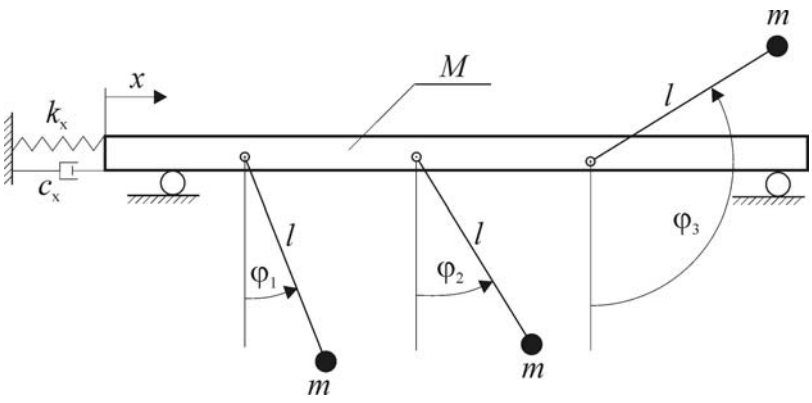

Figure 1: Pendula suspended on the movable beam.

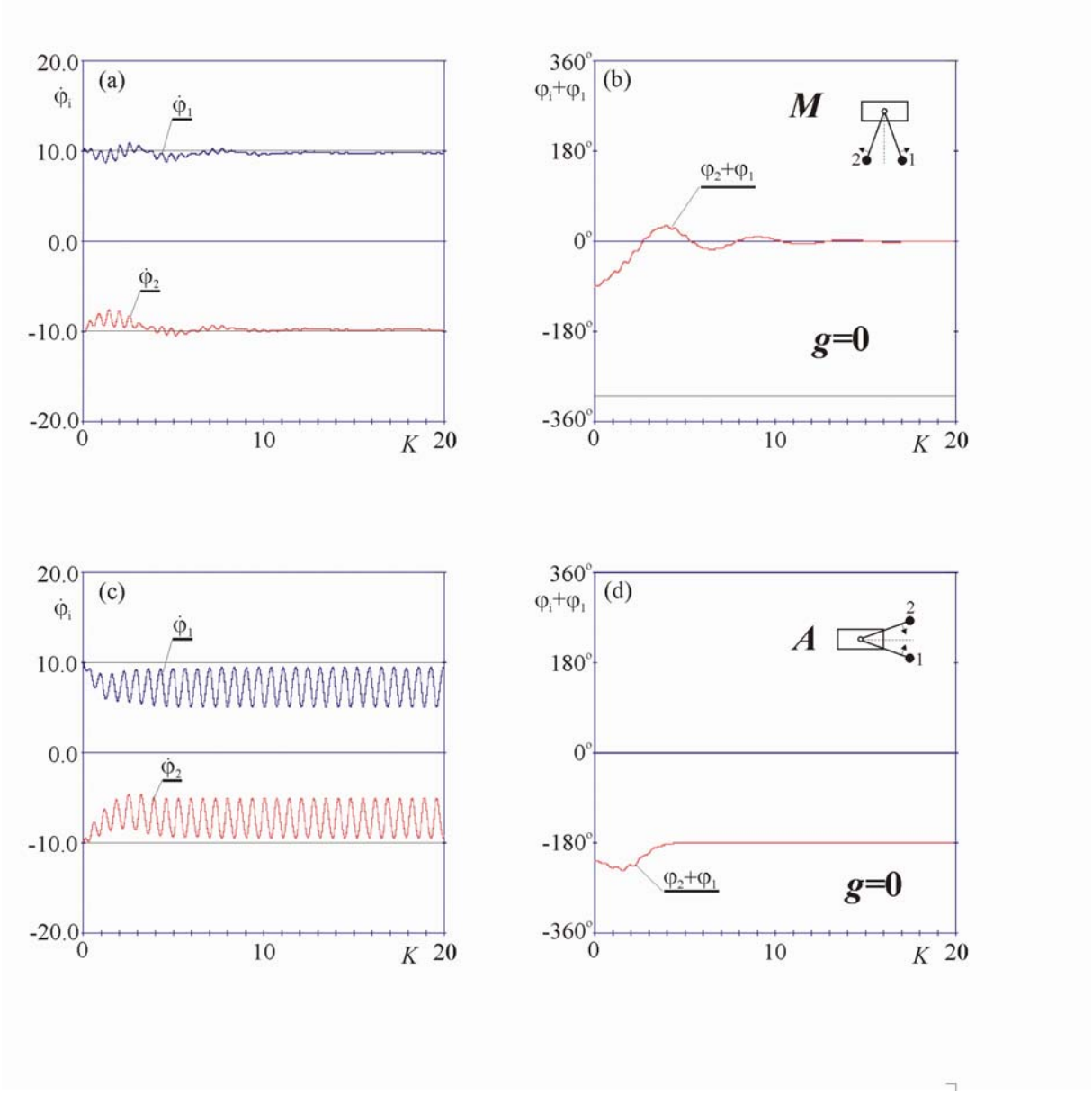

Figure 2. (color online) Mirror-synchronization (*M*) and antiphase-synchronization (*A*) of 2 pendula in the case of the lack of gravity (g=0): (a) pendula's velocities during mirror-synchronization, k_x=500[N/m], $\varphi_{10}=0^o$, $\varphi_{20}=-90^o$; (b) pendula's displacements during mirror-synchronization, k_x=500[N/m], $\varphi_{10}=0^o$, $\varphi_{20}=-90^o$; (c) pendula's velocities during antiphase-synchronization, k_x=500[N/m], $\varphi_{10}=0^o$, $\varphi_{20}=-215^o$; (d) pendula's displacements during antiphase-synchronization, k_x=500[N/m], $\varphi_{10}=0^o$, $\varphi_{20}=-215^o$.

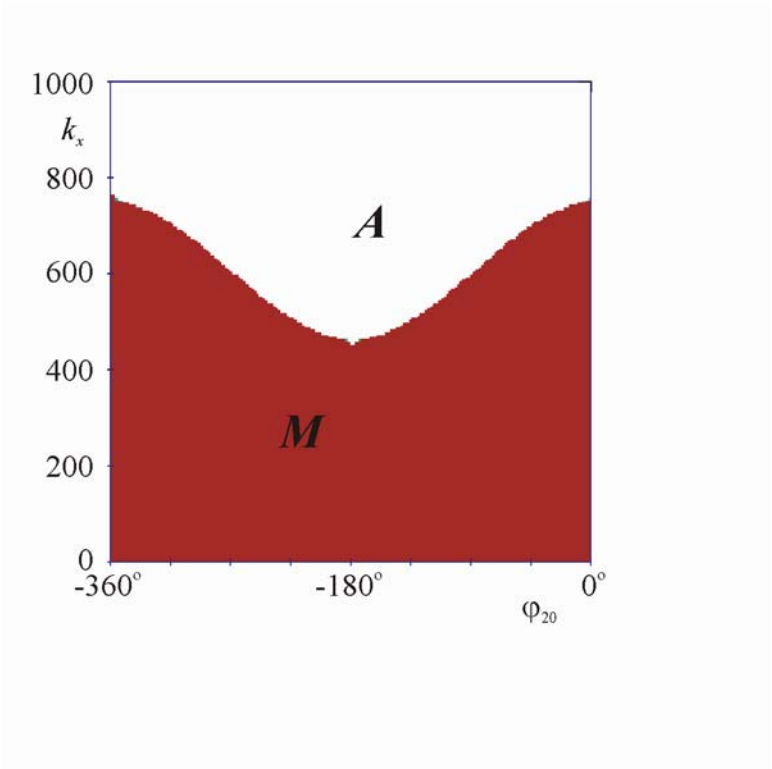

Figure 3: (color online) Type of synchronization of 2 pendula versus stiffness coefficient k_x and initial position of pendulum 2 - φ_{20}, initial positions of pendula 1: $\varphi_{10}=0^o$.

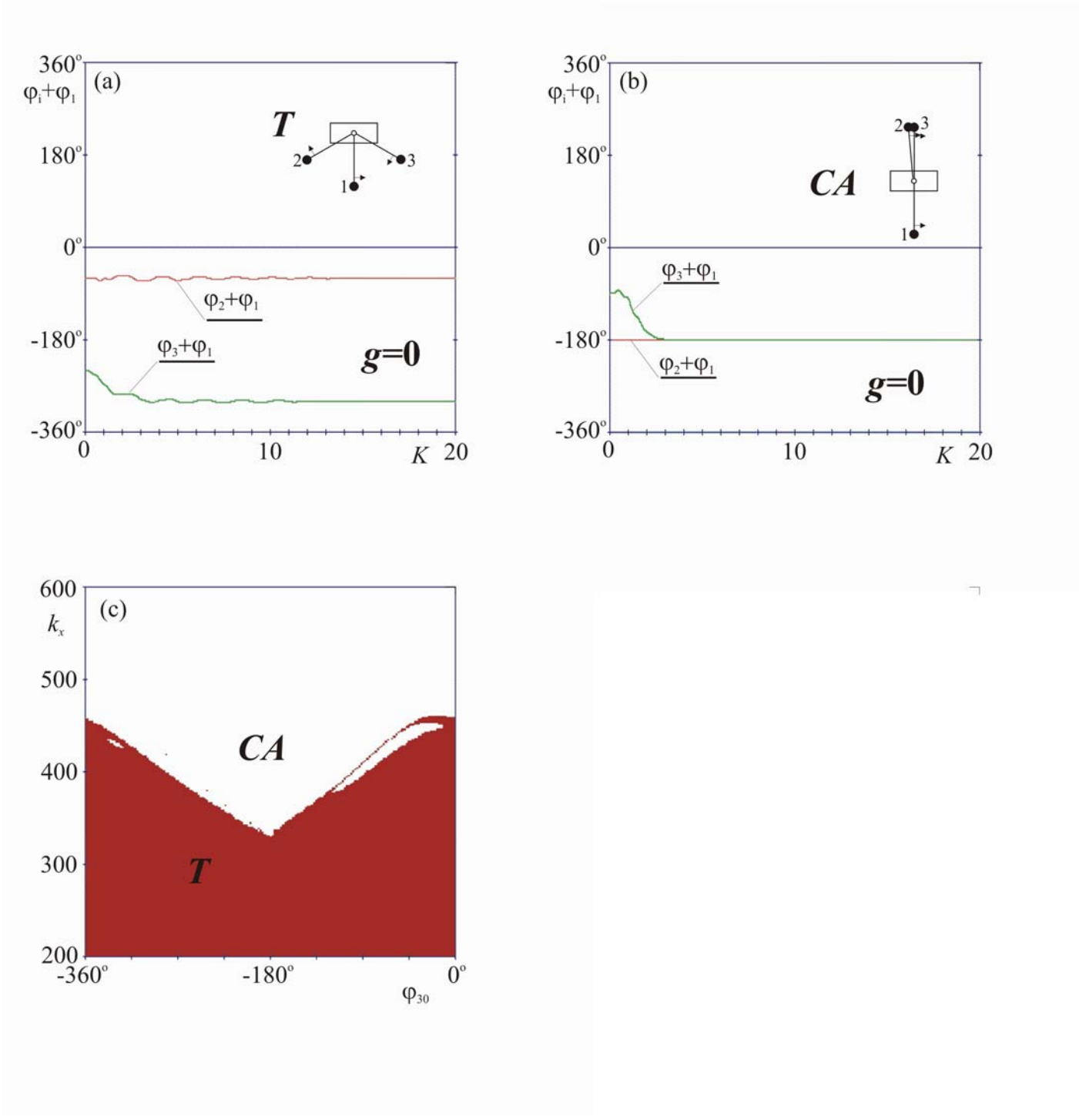

Figure 4. (color online) Different types of synchronization of 3 rotating pendula in the case of lack of gravity (g=0): (a) pendula's displacements during tree-synchronization (T), k_x=200[N/m], φ_{10}=0°, φ_{20}=-60°, φ_{30}=-240°; (b) pendula's displacements during cluster-antiphase-synchronization (CA), k_x=1000[N/m], φ_{10}=0°, φ_{20}=-180°, φ_{30}=-90°; (c) type of synchronization versus stiffness coefficient k_x and initial position of pendulum 3 - φ_{30}, initial positions of pendula 1 and 2: φ_{10}=0°, φ_{20}=-135°;

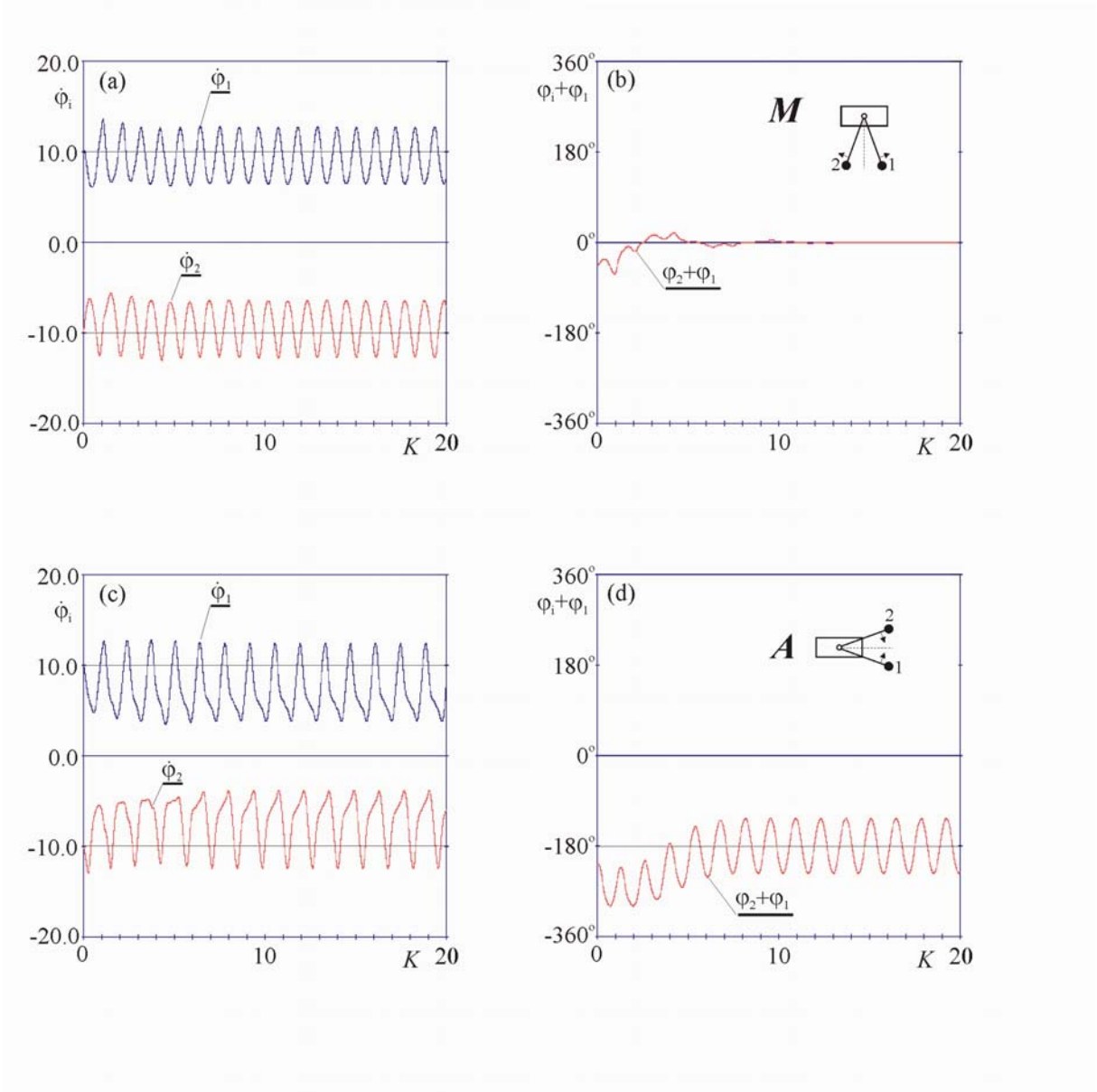

Figure 5: (color online) Mirror-synchronization (*M*) and antiphase-synchronization (*A*) of 2 pendula; (a) pendula's velocities during mirror-synchronization, k_x=500[N/m], φ_{10}=0°, φ_{20}=-45°; (b) pendula's displacements during mirror-synchronization, k_x=500[N/m], φ_{10}=0°, φ_{20}=-45°; (c) pendula's velocities during antiphase-synchronization, k_x=500[N/m], φ_{10}=0°, φ_{20}=-215°; (d) pendula's displacements during antiphase-synchronization, k_x=500[N/m], φ_{10}=0°, φ_{20}=-215°.

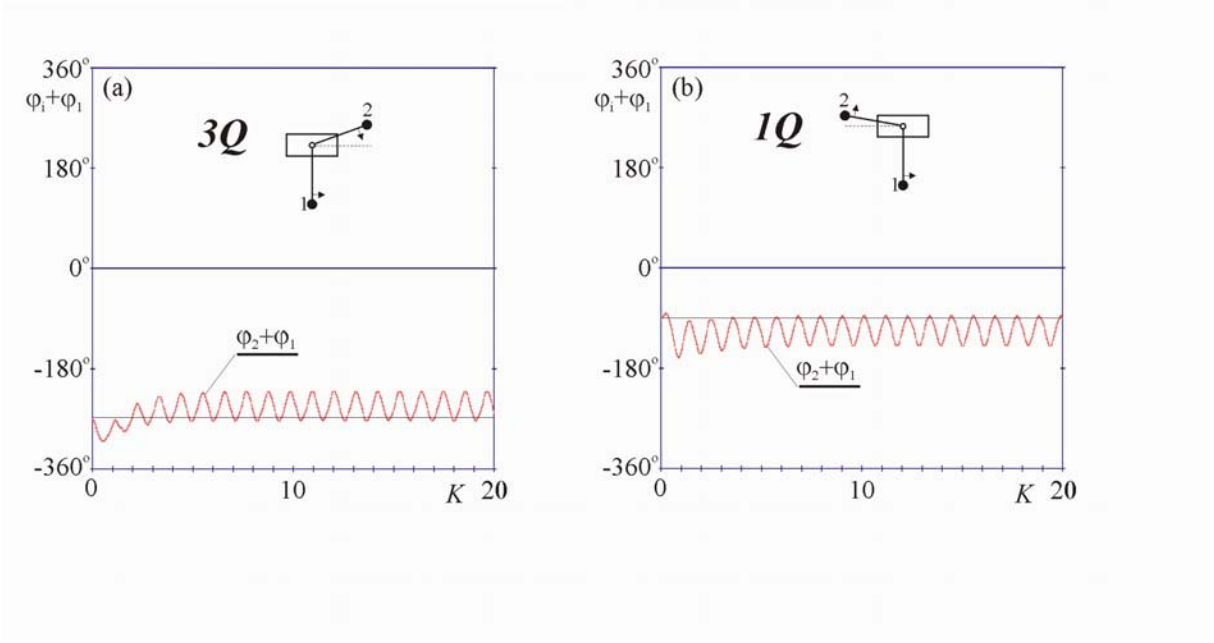

Figure 6: (color online) Third-quarter-synchronization (*3Q*) and first-quarter-synchronization (*1Q*) of 2 pendula; (a) pendula's displacements during third-quarter-synchronization: k_x=3000.0[N/m], φ_{10}=0°, φ_{20}=-270°; (b) pendula's displacements during first-quarter-synchronization: k_x=3000.0[N/m], φ_{10}=0°, φ_{20}=-90°.

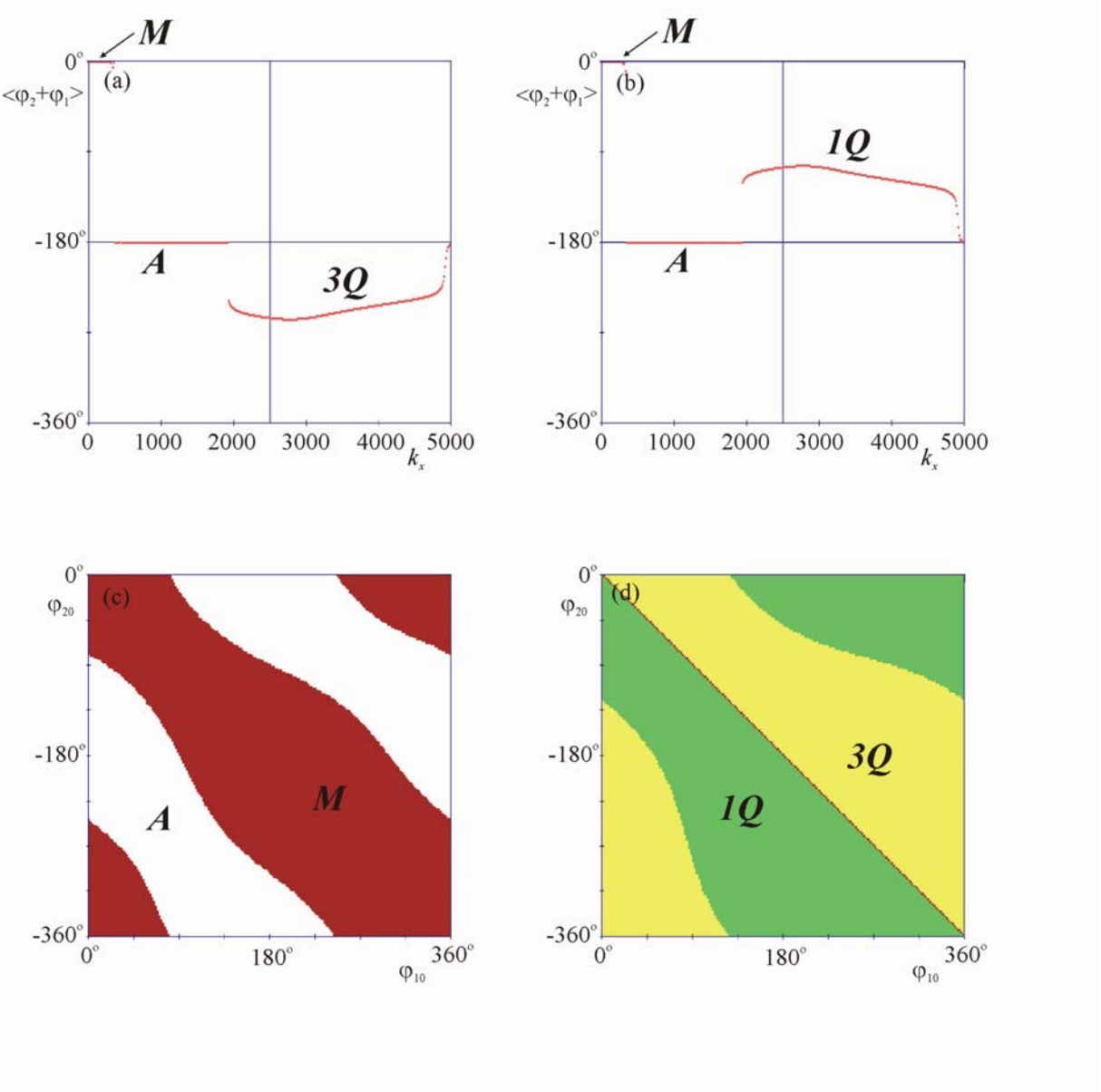

Figure 7: (color online) The influence of the stiffness coefficient k_x on the type of synchronization of 2 pendula: (a) average value of the sum of the pendula's displacements $<\varphi_2+\varphi_1>$ versus k_x: $\varphi_{10}=0^o$, $\varphi_{20}=-270^o$; (b) average value of the sum of the pendula's displacements $<\varphi_2+\varphi_1>$ versus k_x: $\varphi_{10}=0^o$, $\varphi_{20}=-90^o$; (c) mirror- and antiphase-synchronization for different initial conditions: $k_x=500$[N/m]; (d) third- and first- quarter-synchronization for different initial conditions: $k_x=3000$[N/m].

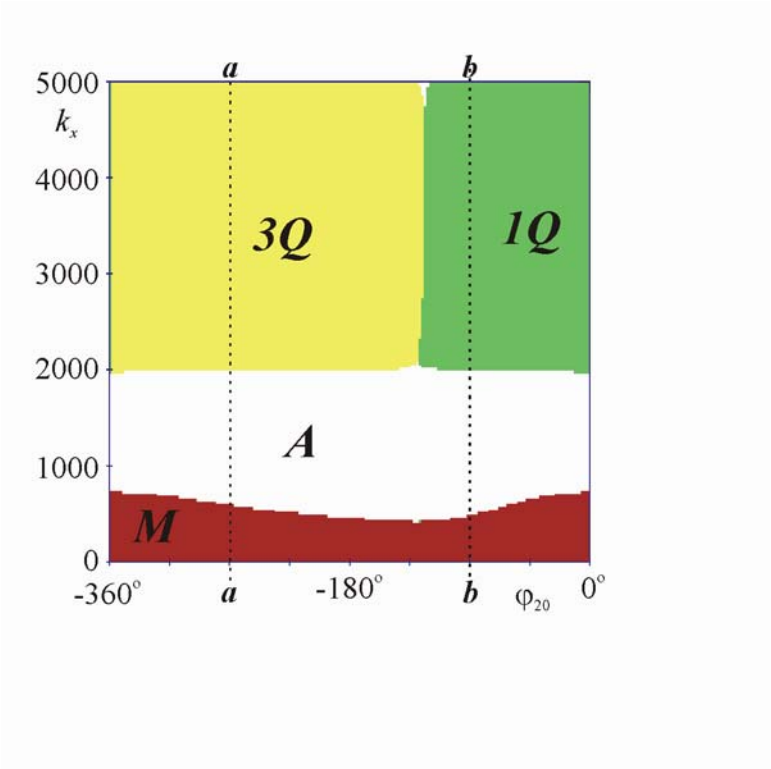

Figure 8. (color online) Different types of synchronization of 2 pendula versus stiffness coefficient k_x and initial position of pendulum 2 φ_{20}: initial position of pendulum 1 $\varphi_{10}=0^o$.

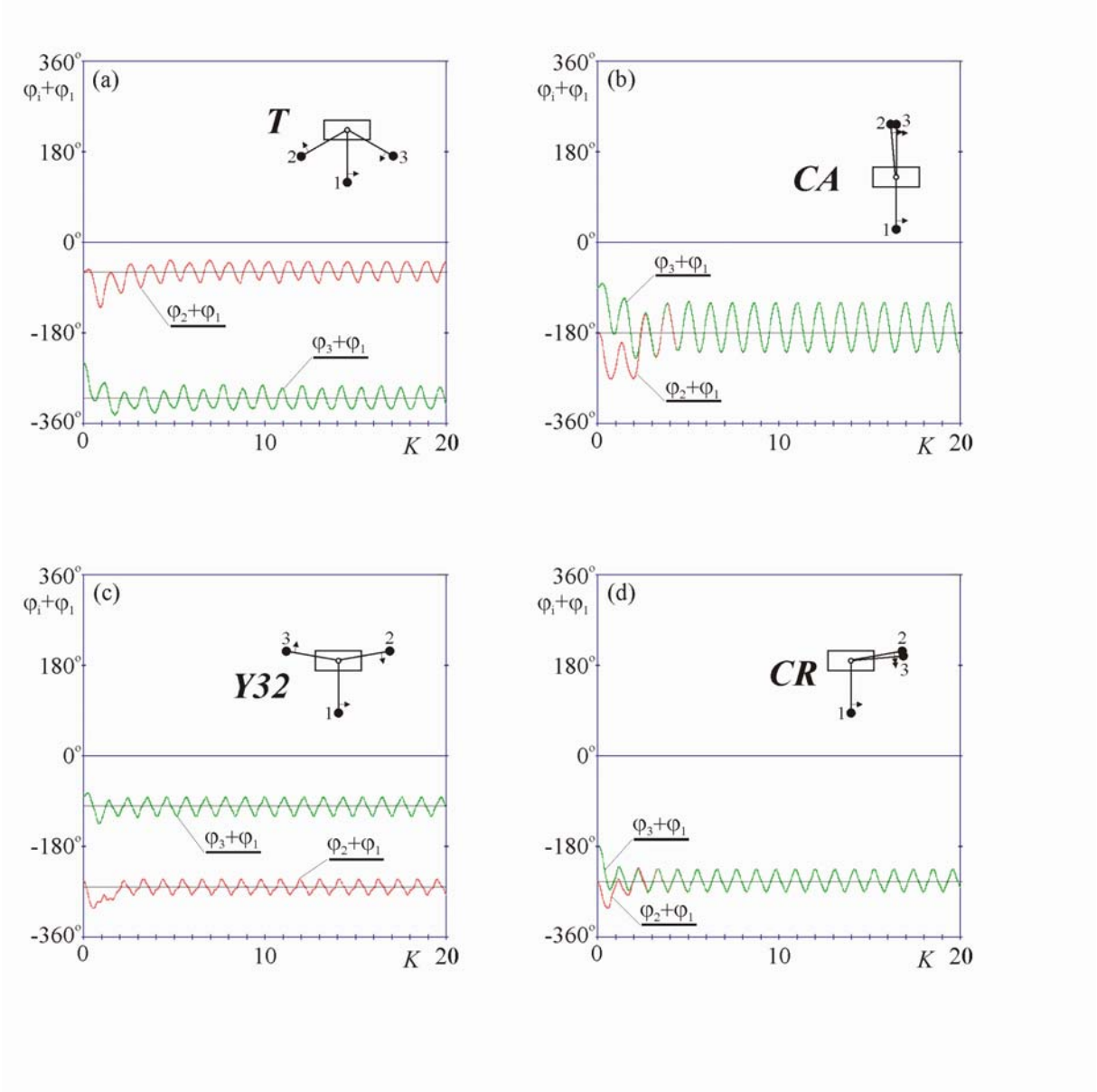

Figure 9: (color online) Different types of synchronization of 3 rotating pendulums: (a) tree synchronization (*T*), k_x=200.0[N/m], φ_{10}=0°, φ_{20}=-60°, φ_{30}=-240°; (b) cluster-antiphase-synchronization (*CA*), k_x=1000.0[N/m], φ_{10}=0°, φ_{20}=-180°, φ_{30}=-90°; (c) yankee-32-synchronization (*Y32*), k_x=3000.0[N/m], φ_{10}=0°, φ_{20}=-250°, φ_{30}=-80°; (d) cluster-right-synchronization (*CR*), k_x=3000.0[N/m], φ_{10}=0°, φ_{20}=-250°, φ_{30}=-180°.

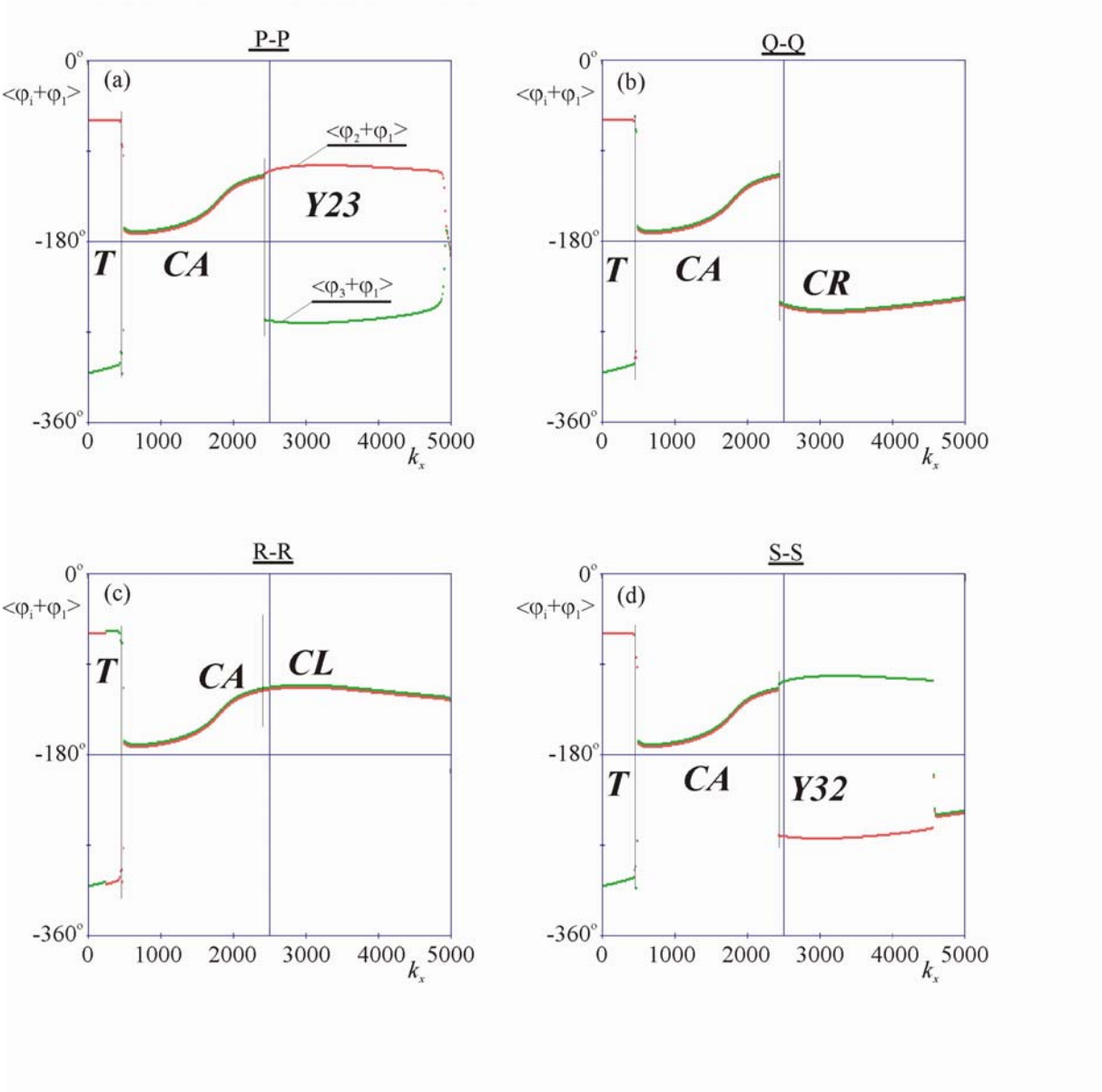

Figure 10: (color online) The influence of the stiffness coefficient k_x on the type of synchronization of 3 pendula shown as the average values of the sums of pendula's displacements $<\varphi_2+\varphi_1>$ and $<\varphi_3+\varphi_1>$ versus k_x: (a) $\varphi_{10}=0^o$, $\varphi_{20}=-135^o$, $\varphi_{30}=-338^o$; (b) $\varphi_{10}=0^o$, $\varphi_{20}=-135^o$, $\varphi_{30}=-180^o$; (c) $\varphi_{10}=0^o$, $\varphi_{20}=-135^o$, $\varphi_{30}=-80^o$; (d) $\varphi_{10}=0^o$, $\varphi_{20}=-135^o$, $\varphi_{30}=-40^o$.

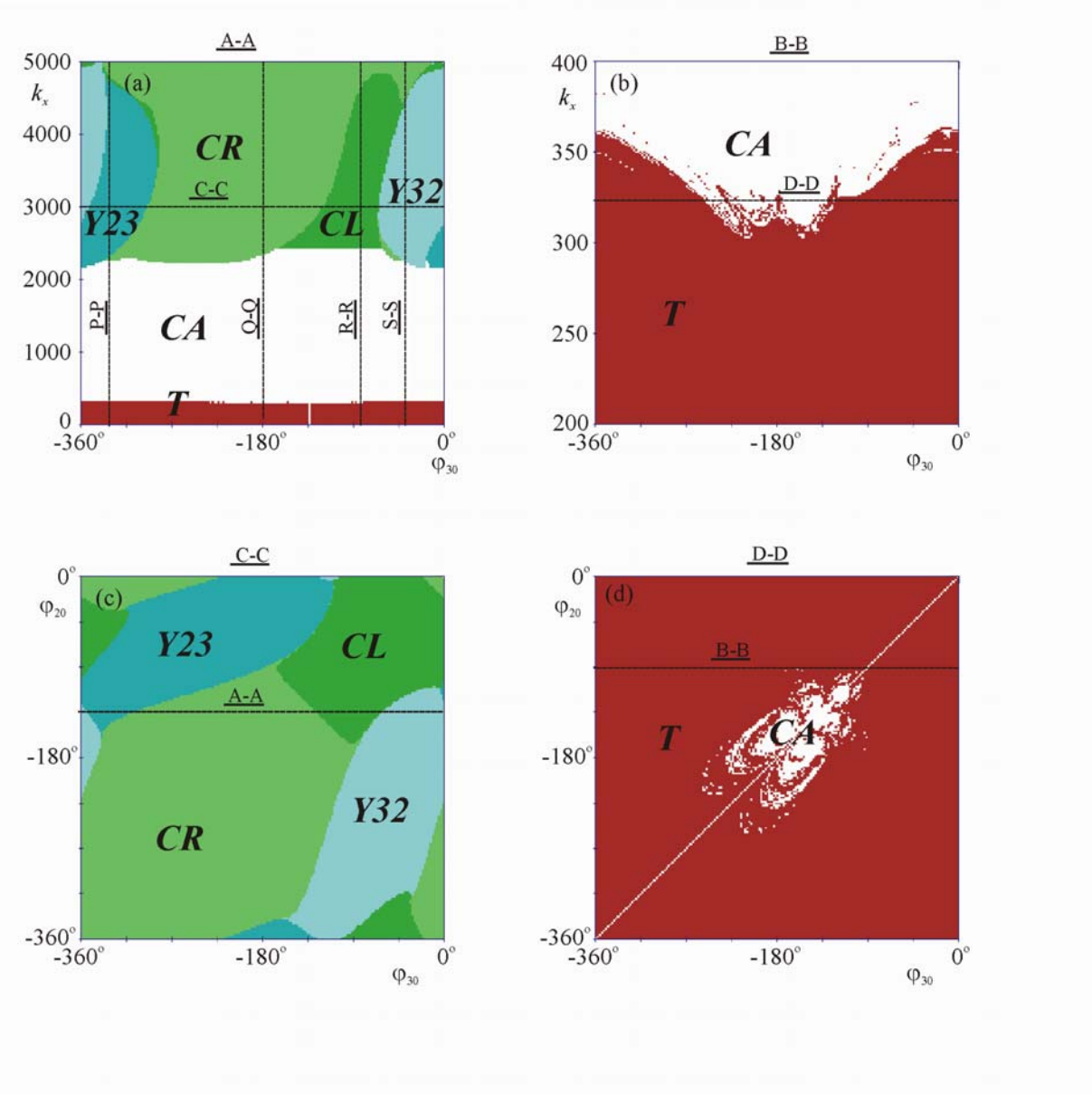

Figure 11: (color online) Dependence of the type of synchronization on the stiffness ratio k_x and initial conditions: (a) type of synchronization versus k_x and φ_{30}: φ_{10}=0°, φ_{20}=-135°; A-A cross-section of map (c); (b) the enlargement of map (a) for small values of k_x, B-B cross-section map (d); (c) the type of synchronization for different initial conditions φ_{20} and φ_{30}; φ_{10}=0°, k_x=3000 [N/m], C-C cross-section map (a); (d) the type of synchronization as function φ_{20} and φ_{30}; φ_{10}=0°, k_x = 325[N/m], D-D cross-section map (b).

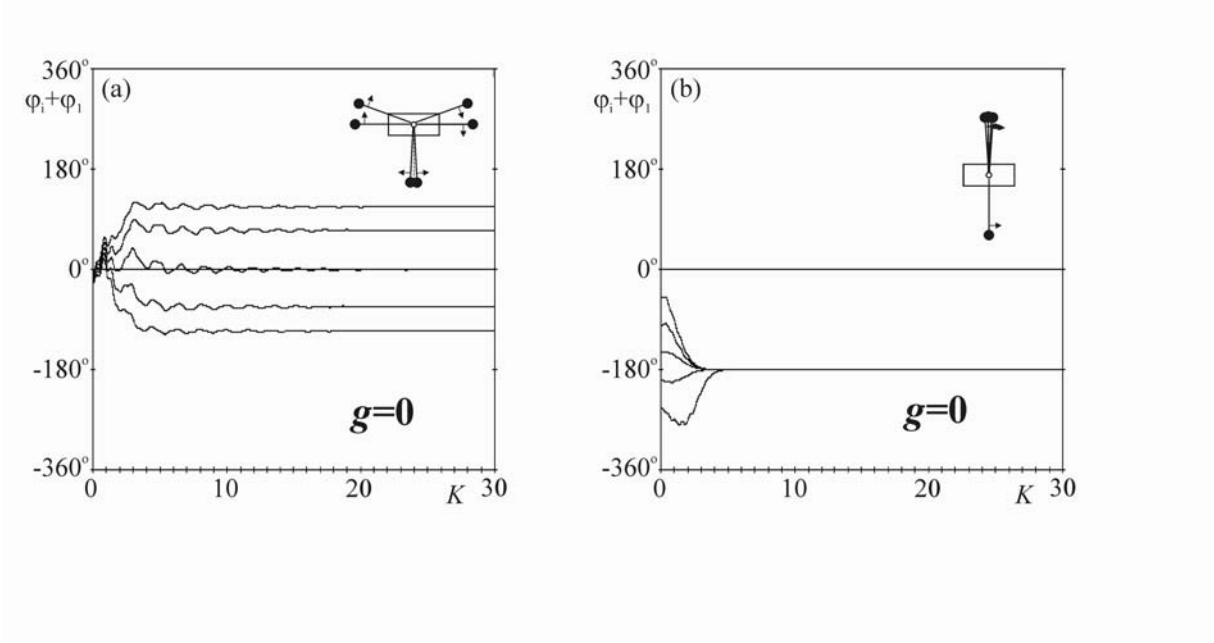

Figure 12: Tree-synchronization (*M*) and antiphase-synchronization (*A*) of six pendula rotating in horizontal plane (lack of gravity: g=0); (a) pendula's displacements during the tree-synchronization, k_x=200.0[N/m], φ_{10}=0.0°, φ_{20}=-5.0°, φ_{30}=-10.0°, φ_{40}=-15.0°, φ_{50}=-20.0°, φ_{60}=-25.0°, (b) pendula's displacements during the cluster-antiphase-synchronization, k_x=2000.0[N/m], φ_{10}=0.0°, φ_{20}=-50.0°, φ_{30}=-100.0°, φ_{40}=-150.0°, φ_{50}=-200.0°, φ_{60}=-250.0°.

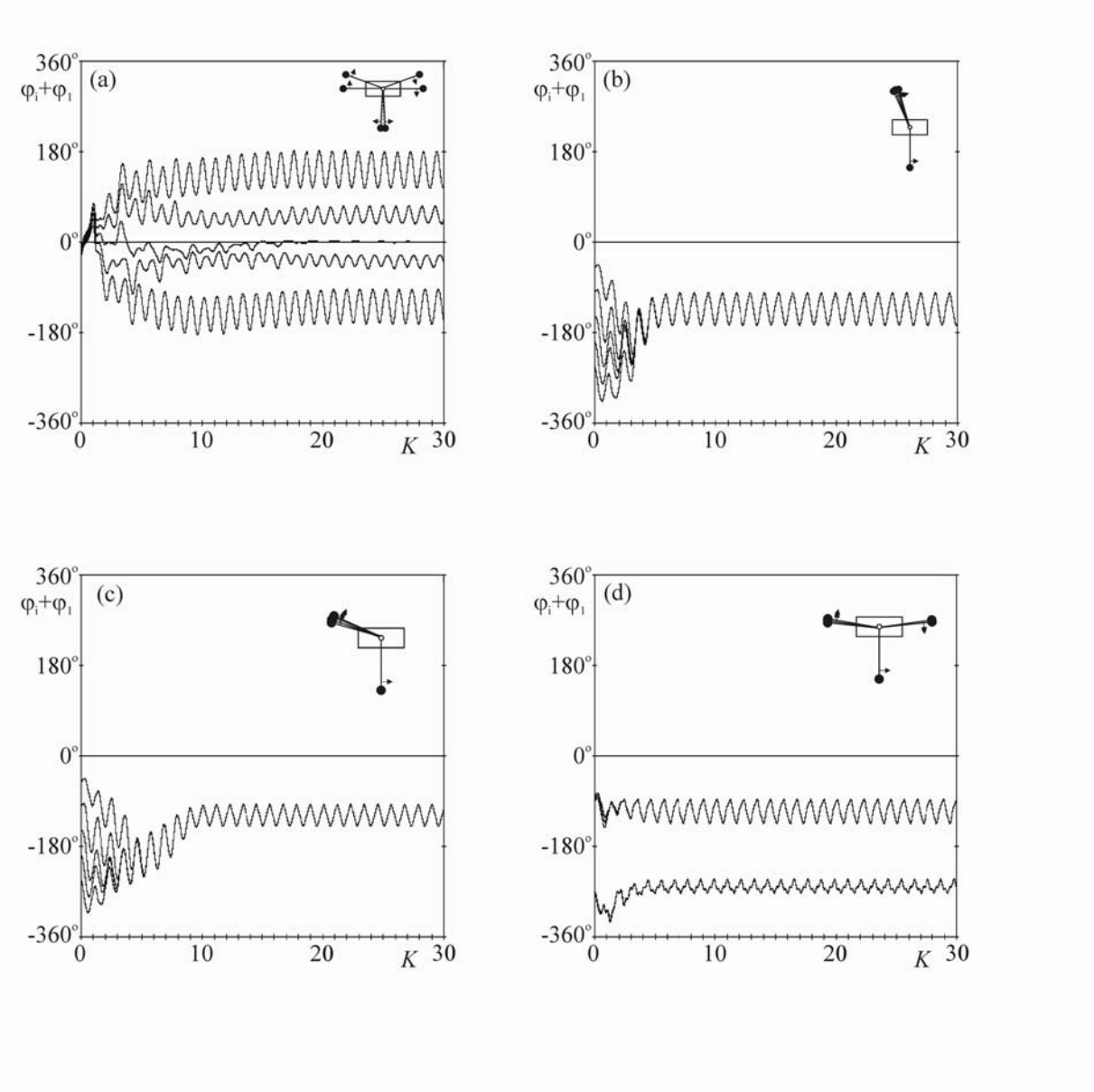

Figure 13: Different types of synchronization for the system with six pendulums in gravitational field (g=9.81[m/s^2]); (a) pendula's displacements during the tree-synchronization, k_x=200.0[N/m], φ_{10}=0.0^o, φ_{20}=-5.0^o, φ_{30}=-10.0^o, φ_{40}=-15.0^o, φ_{50}=-20.0^o, φ_{60}=-25.0^o, (b) pendula's displacements during the cluster-antiphase-synchronization, k_x=2000.0[N/m], φ_{10}=0.0^o, φ_{20}=-50.0^o, φ_{30}=-100.0^o, φ_{40}=-150.0^o, φ_{50}=-200.0^o, φ_{60}=-250.0^o, (c) pendula's displacements during the cluster-left-synchronization, k_x=3000.0[N/m], φ_{10}=0.0^o, φ_{20}=-50.0^o, φ_{30}=-100.0^o, φ_{40}=-150.0^o, φ_{50}=-200.0^o, φ_{60}=-250.0^o, (d) pendula's displacements during the yankee-synchronization, k_x=3000.0[N/m], φ_{10}=0.0^o, φ_{20}=-80.0^o, φ_{30}=-85.0^o, φ_{40}=-90.0^o, φ_{50}=-270.0^o, φ_{60}=-275.0^o.

n	Type of synchronization and conditions for its occurrence
2	*Mirror synchronization*- Figure 2(b) (g=0.0) and Figure 5(b) (g=9.81[m/s^2]): $\varphi_1 = \omega t + \eta \sin \omega t, \varphi_2 = -\omega t + \eta \sin(-\omega t)$, $\varphi_1+\varphi_2=0$.
2	*Antiphase synchronization*- Figure 2(d) (g=0.0) and Figure 5(d) (g=9.81[m/s^2]): $\varphi_1 = \omega t + \eta \sin \omega t, \varphi_2 = -\omega t - 180^\circ + \eta \sin(-\omega t - 180^\circ)$, $\varphi_1+\varphi_2=180^\circ+2\eta\sin\omega t$.
2	*3Q synchronization*- Figure 6(a) – exists only in the case when pendula rotate in the vertical plane: $\varphi_1 = \omega t + \eta \sin \omega t,\ \varphi_2 = -\omega t - \beta_{3Q} + \eta \sin(-\omega t - \beta_{3Q})$, $\varphi_1 + \varphi_2 = -\beta_{3Q} + \eta(1 - \cos \beta_{3Q}) \sin(\omega t) - \eta \sin \beta_{3Q} \cos(\omega t)$, $\beta_{3Q} \in [-270^\circ,-180^\circ]$ (exact value depends on the value of k_x).
2	*1Q synchronization*- Figure 6(a) – exists only in the case when pendula rotate in the vertical plane. $\varphi_1 = \omega t + \eta \sin \omega t, \varphi_2 = -\omega t - \beta_{1Q} + \eta \sin(-\omega t - \beta_{1Q})$, $\varphi_1 + \varphi_2 = -\beta_{1Q} + \eta(1 - \cos \beta_{1Q}) \sin(\omega t) - \eta \sin \beta_{1Q} \cos(\omega t)$, $\beta_{1Q} \in [-180^\circ,-90^\circ]$ (exact value depends on the value of k_x).
3	*Tree synchronization* – Figure 4(a) (g=0.0) and Figure 9(a) (g=9.81[m/s^2]). $\varphi_1 = \omega t + \eta \sin \omega t$, $\varphi_2 = -\omega t - 60^\circ + \eta \sin(-\omega t - 60^\circ)$, $\varphi_3 = -\omega t - 300^\circ + \eta \sin(-\omega t - 300^\circ)$, $\varphi_1 + \varphi_2 = -60^\circ + \eta(1 - \cos 60^\circ) \sin \omega t - \eta \sin 60^\circ \cos \omega t$, $\varphi_1 + \varphi_3 = -300^\circ + \eta(1 - \cos 300^\circ) \sin \omega t - \eta \sin 300^\circ \cos \omega t$.
3	*Cluster-antiphase synchronization* – Figure 4(b) (g=0.0) and Figure 9(b) (g=9.81[m/s^2]). $\varphi_1 = \omega t + \eta \sin \omega t$, $\varphi_2 = -\omega t - \beta_{CA} + \eta \sin(-\omega t - \beta_{CA})$, $\varphi_3 = -\omega t - \beta_{CA} + \eta \sin(-\omega t - \beta_{CA})$, $\varphi_1 + \varphi_2 = -\beta_{CA} + \eta(1 - \cos \beta_{CA}) \sin \omega t - \eta \sin \beta_{CA} \cos \omega t$, $\varphi_1 + \varphi_3 = -\beta_{CA} + \eta(1 - \cos \beta_{CA}) \sin \omega t - \eta \sin \beta_{CA} \cos \omega t$. For g=0 and η=0 the angle β_{CA} is equal to 180° and for g=9.81[m/s^2] the angle β_{CA} is in the range $-180^\circ<\beta_{CA}<-90^\circ$ depending on the value of k_x.
3	*Cluster right synchronization* – Figure 9(d) – exists only in the case when pendula rotate in the vertical plane. $\varphi_1 = \omega t + \eta \sin \omega t$, $\varphi_2 = -\omega t - \beta_{CR} + \eta \sin(-\omega t - \beta_{CR})$, $\varphi_3 = -\omega t - \beta_{CR} + \eta \sin(-\omega t - \beta_{CR})$, $\varphi_1 + \varphi_2 = -\beta_{CR} + \eta(1 - \cos \beta_{CR}) \sin \omega t - \eta \sin \beta_{CR} \cos \omega t$, $\varphi_1 + \varphi_3 = -\beta_{CR} + \eta(1 - \cos \beta_{CR}) \sin \omega t - \eta \sin \beta_{CR} \cos \omega t$, where the angle β_{CR} is close to $\beta_{CR}=-270^\circ$ (the exact value depends on k_x).
3	*Cluster left synchronization* The same conditions as for cluster right synchronization. Replace the angle β_{CR} by the angle β_{CL} which is close to $\beta_{CL}=-90^\circ$ (the exact value depends on k_x).
3	*Yankee 32 synchronization* – Figure 9(c)

	$\varphi_1 = \omega t + \eta \sin \omega t,$ $\varphi_2 = -\omega t - \beta_{Y2} + \eta \sin(-\omega t - \beta_{Y2}),$ $\varphi_3 = -\omega t - \beta_{Y3} + \eta \sin(-\omega t - \beta_{Y3}),$ $\varphi_1 + \varphi_2 = -\beta_{Y2} + \eta(1 - \cos \beta_{Y2}) \sin \omega t - \eta \sin \beta_{Y2} \cos \omega t,$ $\varphi_1 + \varphi_3 = -\beta_{Y3} + \eta(1 - \cos \beta_{Y3}) \sin \omega t - \eta \sin \beta_{Y3} \cos \omega t,$ where the angle β_{Y2} is β_{Y2}=-90^o, and the angle β_{Y3} is close β_{Y3}=-270^o (the exact values depend on k_x).
3	*Yankee 23 synchronization* The same conditions as for the Yankee Y32 synchronization but pendula 2 and 3 are changing positions between themselves.

Table 1. Types of synchronization of n=2,3 pendula and the conditions for their occurrence. The harmonic component $\eta \sin \omega t$ describes the influence of the gravity of the pendula's rotation (when pendula rotate in horizontal plane η=0).